

## Influence of surface mechanical attrition treatment (SMAT) on oxidation behavior of 316L stainless steel at 650°C

S. Benafia <sup>1, a\*</sup>, D. Retraint <sup>1, b</sup>, B. Panicaud <sup>1, c</sup> J.L Grosseau Poussard <sup>2, d</sup>

<sup>1</sup> Charles Delaunay Institute, LASMIS, UMR STMR CNRS 6279, University of Technology of Troyes, 10000 Troyes, France

<sup>2</sup> LaSIE FRE-CNRS 3474, Pôle Sciences et Technologie, Université de La Rochelle, Av. M. Crépeau, 17042 La Rochelle Cedex, France

<sup>a</sup> souhail.ben\_afia@utt.fr, <sup>b</sup> delphine.retraint@utt.fr, <sup>c</sup> benoit.panicaud@utt.fr, <sup>d</sup> jlgrouss@univ-lr.fr

**Keywords:** High-temperature oxidation; Stress measurements; Creep relaxation; Residual stresses; Chromium oxide, SMAT, nanocrystallisation

### Abstract

In this paper, the effects of Surface Mechanical Attrition Treatment on the high-temperature oxidation of AISI 316L austenitic stainless steel are investigated. Samples treated with different conditions were oxidized at 650°C in order to study the effect of this type of nanocrystallisation on the oxidation resistance of the alloy concerned. X-ray diffraction and in-situ Raman spectroscopy were used to identify the oxides formed at the surface. The results indicate the presence of hematite and chromium oxides. Experimental results obtained by Raman spectroscopy were also used to study the stress evolution in Cr<sub>2</sub>O<sub>3</sub> films during isothermal conditions.

### Introduction

Surface Mechanical Attrition Treatment (SMAT) is a recent process that enables to nanocrystallise the surface of metallic alloys. It can enhance the mechanical properties of the treated material by inducing a grain refinement down to the nanometer scale in the top surface layer. This nanocrystallisation process leads to different effects that were successively studied on several metallic materials [1]. Recently, some investigations have been performed on these effects; most of them mainly focus on the surface morphologies and tribological properties [2]. Nevertheless SMAT is expected to affect the oxidation resistance. Indeed, due to induced grain size refinement, an increase of the grain boundary fraction from the core of the sample to the top surface may modify the diffusion mechanisms. It is now well established that the surface reactivity can be modified by nanocrystallisation treatment [3]. Moreover, the presence of residual stresses in thermal oxide layers during the isothermal oxidation process may influence the protective properties of the oxide layers. In the present work, the effects of SMAT on the oxidation behavior of a 316L stainless steel are specifically investigated at 650°C. This stainless steel is widely used in various sectors of industry due to its high mechanical strength and generally good oxidation resistance at high temperature [4]. In the first section of the present paper, the oxidation mechanisms occurring in metal/oxide systems and phase evolution are investigated using thermogravimetric analyses, X-ray diffraction and in-situ Raman spectroscopy measurements. The latter technique is used to experimentally study the residual stresses in Cr<sub>2</sub>O<sub>3</sub> films, and allows the determination of thermal and growth stresses. Finally, the mechanisms involved are analysed in order to understand how SMAT may affect the oxidation resistance of 316L stainless steel.

## Material and surface treatment and oxidation

3 mm thick AISI 316L samples are cut from 35 mm diameter bars and treated with the nanocrystallisation process SMAT. Fig. 1 shows a simple geometrical representation of the process. During the treatment, a spherical shot is set in motion by a high frequency (20 kHz) ultrasonic generator. Random shot impacts at the sample surface generate severe plastic deformations so that a superficial nanocrystalline layer is formed [5]. This process takes place in air at room temperature, during 20 minutes on each main surface (symmetric treatment). Suitable SMAT parameters such as processing time and shot size (3 mm) are chosen based on previous experiments. An intermediary mechanical polishing step is carried out to remove a thin superficial layer of  $3\pm 0.3\text{ }\mu\text{m}$ . Moreover, after nanocrystallisation treatment, oxidation under different temperatures has been investigated. This paper focuses on the case performed at  $650^\circ\text{C}$  in ambient air during an oxidation time of 20 h. This temperature is carefully investigated according to common applications of 316L. This choice also allows observing the impact of SMAT technique on the oxidation properties. Indeed, if oxidation temperature is above  $750^\circ\text{C}$ , grain growth may occur and lead to the disappearance of nanocrystals.

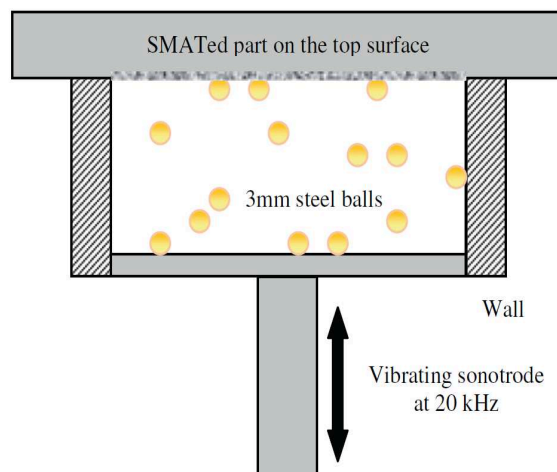


Figure 1 Geometrical representation of the SMAT process

## SMAT chemical effects on oxidation resistance at $650^\circ\text{C}$

### Experimental techniques

Oxidation of the 316L stainless steel has been studied using several techniques. First, the problem is considered from a chemical and macroscopic point of view. A classical thermogravimetric analysis in a Setaram TGA 92 thermobalance has thus been used. Samples are heated at  $50^\circ\text{C}/\text{min}$  up to the desired oxidation temperature of  $650^\circ\text{C}$ . The selected temperature is supposed to be stable after 1000s within the range  $\pm 0.1^\circ\text{C}$ . The in-situ characterization of the oxide scales is carried out in a high temperature chamber adapted on a high resolution XY Raman spectrometer equipped with a CCD detector. Its wavenumber precision  $\Delta\nu$  Raman is equal to  $0.1\text{ cm}^{-1}$ . The stimulation source is a helium–neon laser ( $\lambda = 632.817\text{ nm}$ ). The crystal structure is analyzed by X-ray diffraction (XRD) with a Seifert PTS-3000 X-ray diffractometer using  $\text{CuK}\alpha$  radiation and Bragg–Brentano conditions, directly on the sample surface.

### Kinetics results

The weight change curves (per unit of surface) as a function of the oxidation time are shown in Fig. 2, for both treated (blue line) and untreated (red line) specimens. Two stages are observed: first a linear stage, and then after a breakaway a more or less parabolic stage. The parabolic regime of the untreated 316L curve is characterized by a rate constant  $k_{\text{MP}} = 7.03 \cdot 10^{-12}\text{ kg}^2\text{ m}^{-4}\text{ s}^{-1}$ . Such parabolic

results are coherent with other works for untreated stainless steel materials [6]. The  $k_{MP}$  value for the treated 316L curve is found equal to  $2.77 \cdot 10^{-11} \text{ kg}^2 \text{ m}^{-4} \text{ s}^{-1}$ , which correspond to a relative increase of 35%. Consequently, and regardless to the chosen data processing method, experiments show that SMAT leads to an intensification of 316L degradation during high temperature oxidation at  $650^\circ\text{C}$  after 20 h.

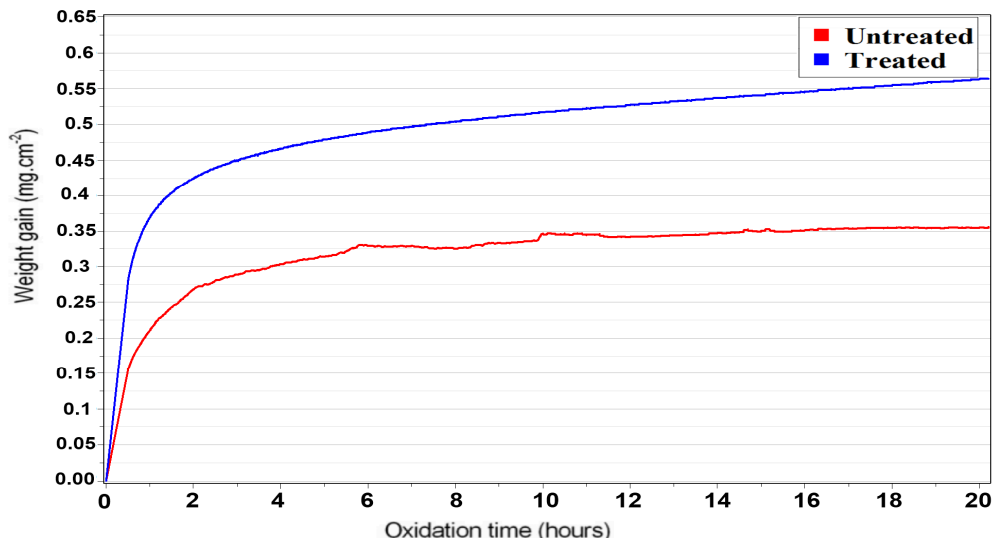


Figure 2 Mass change of untreated and treated 316L, during isothermal oxidation at  $650^\circ\text{C}$  in air

### Oxide phases composition

In order to complete the previous experimental observations, the composition of the oxide layer is studied by XRD. Fig. 3 represents XRD analyses in the conventional  $\theta$ - $2\theta$  mode, for the treated and untreated specimens after oxidation process. Two indexed Raman spectra are also presented in Fig. 4, which is only a qualitative illustration of the phase actually present within the oxide layer (at the particular instant of the measurement, after 2h and 20h). Fig. 4 shows differences between Raman spectra of treated and untreated samples. For short oxidation periods (2h), the only oxide observed is  $\text{Fe}_2\text{O}_3$ , for both specimens. For longer exposure times (20h), different oxides are found such as  $\text{Fe}_2\text{O}_3$ ,  $\text{Fe}_3\text{O}_4$  and  $\text{Cr}_2\text{O}_3$ , for both specimens.

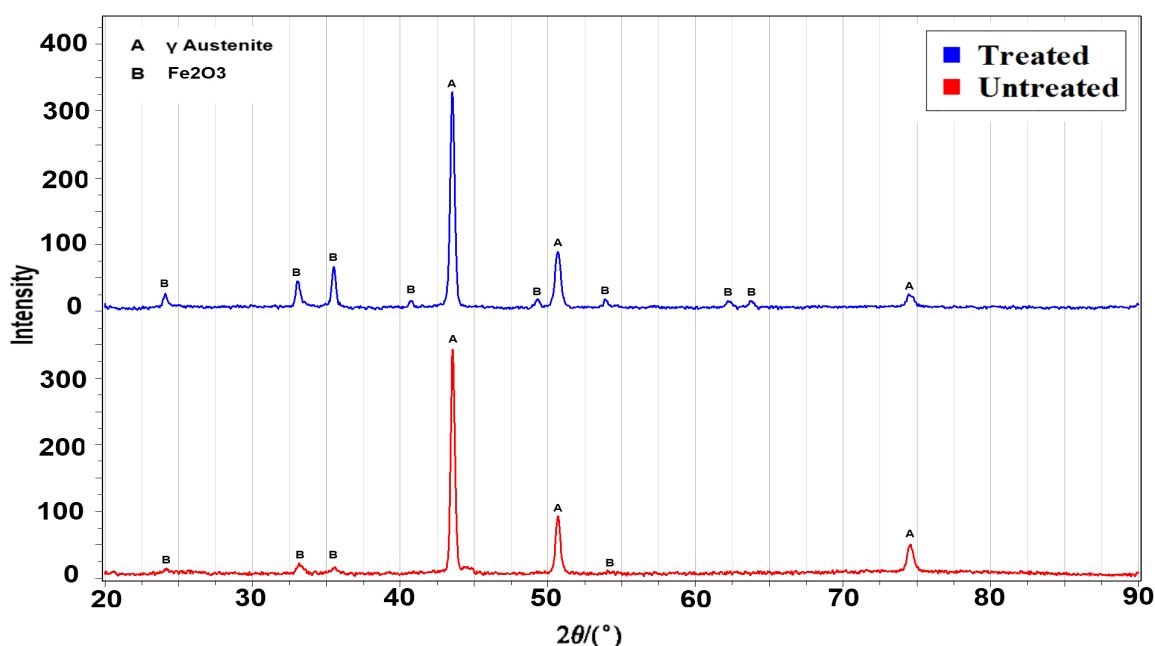


Figure 3 X-ray diffractograms obtained for untreated and treated samples.

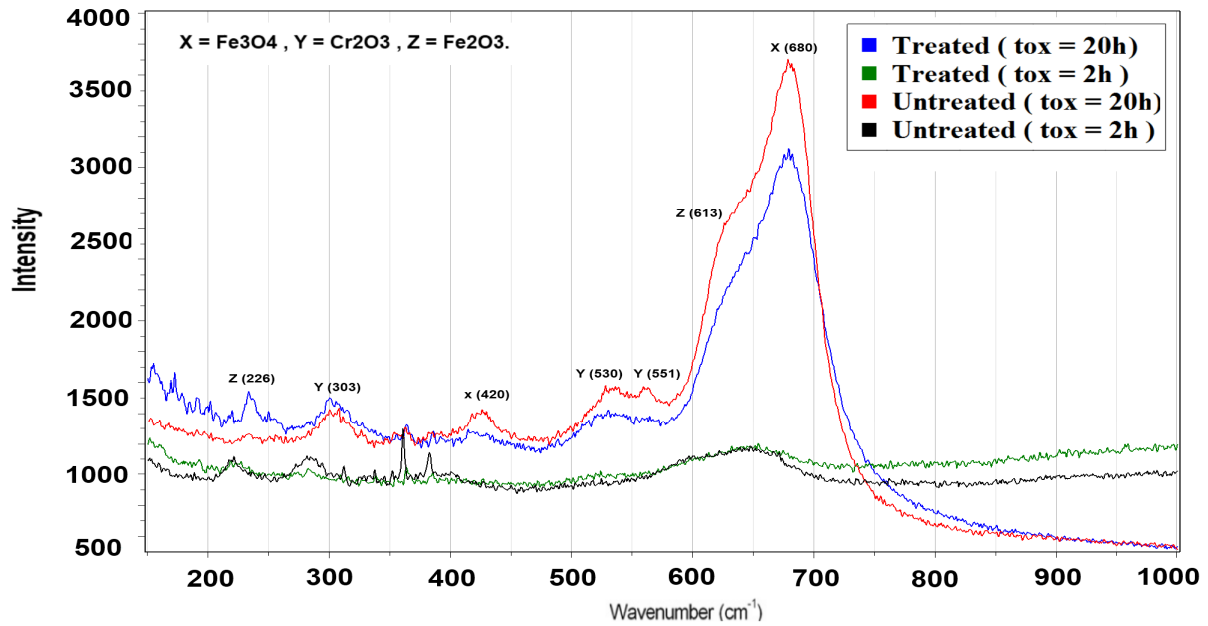


Figure 4 Intensity versus wavenumber. Raman spectra of untreated and SMATed specimens, for two different times (2 h and 10 h).

The X-ray diffractogram shows (Fig. 3, corresponding to ambient measurement after 20 h) that the treated and oxidized specimens are mainly constituted of  $\text{Fe}_2\text{O}_3$  oxide. Analysing the diffractograms with Maud program, it was possible to better exploit XRD measurements and extract the percentages of phases. The analyzed zone of the untreated sample contains 36%  $\text{Fe}_2\text{O}_3$ , 6%  $\text{Cr}_2\text{O}_3$  and 58% austenite. The treated sample contains 22%  $\text{Fe}_2\text{O}_3$ , 3%  $\text{Cr}_2\text{O}_3$ , 4%  $\text{Fe}_3\text{O}_4$  and 69% austenite. These results confirm the protective character of chromium oxide reflecting the better oxidation resistance of the untreated sample. The selective oxidation of chromium could be correlated with the formation of the fine-grain structure on the surface region of the treated sample. In the next part, this work will focus on the stress evolution with oxidation time related to the oxidation kinetics.

### SMAT mechanical effects on oxidation resistance at 650°C

Deformations have been measured using the micro-Raman spectrometer previously described. Three peaks from the chromium oxide layer are specially investigated in each Raman spectrum, corresponding to the following three vibrations modes; two Bg and one Ag [7]. In Fig. 4, these three peaks are indexed according to their wavenumber at room temperature. The experimental stresses within the global oxide films are studied particularly in the  $\text{Cr}_2\text{O}_3$  phase; it is limited to chromium oxide and other phases are not studied. Thus, by using pseudo-Voigt fitting (with Lab-Spec software), the corresponding wavenumber  $\nu$  is deduced as a function of the oxidation time (Fig.5). Besides, in order to calibrate this methodology, the stress-free state is required. The evolution of the stress-free wavenumber with the temperature has been obtained for the considered modes at different temperatures from the literature [7]. The corresponding stress-free reference spectrum at 650°C is deduced making it possible to determine the stress in the constrained oxide from the variation of the wavenumber with respect to this reference. The variation  $\Delta\nu$  for each mode is used to deduce the corresponding stress  $\sigma$  (with  $\Delta\nu = \nu(T, \sigma) - \nu(T, 0)$  where  $\nu(T, \sigma)$  and  $\nu(T, 0)$  are, respectively, the wavenumbers for constrained and unstressed oxides at the working temperature T). According to Mougin [7], the following stress dependency of the  $\Delta\nu$  wavenumber was thus calculated for the peak at 551  $\text{cm}^{-1}$ :

$$\Delta\sigma_{ox} = -0.307 \Delta\nu \pm 120 \text{ MPa} \quad (1)$$

Where  $\sigma_{ox}$  is expressed in GPa and  $\Delta\nu$  in  $\text{cm}^{-1}$ .

Stress evolutions for untreated and treated samples are presented in Fig. 6.

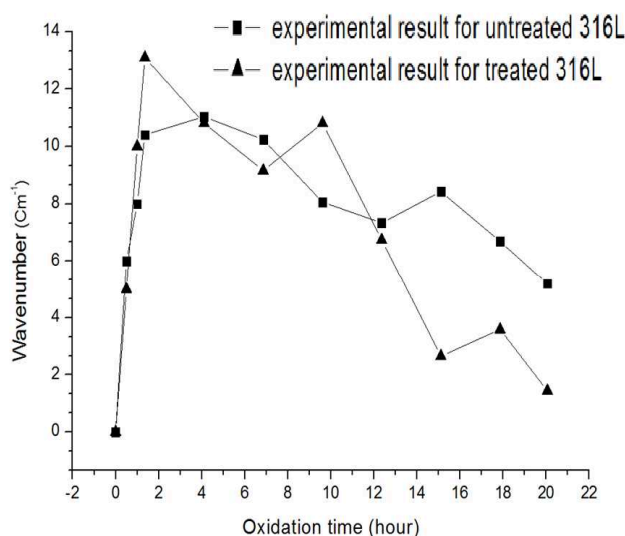


**Figure 5** Wavenumber evolution of  $\text{Cr}_2\text{O}_3$  peaks (551) versus oxidation time.

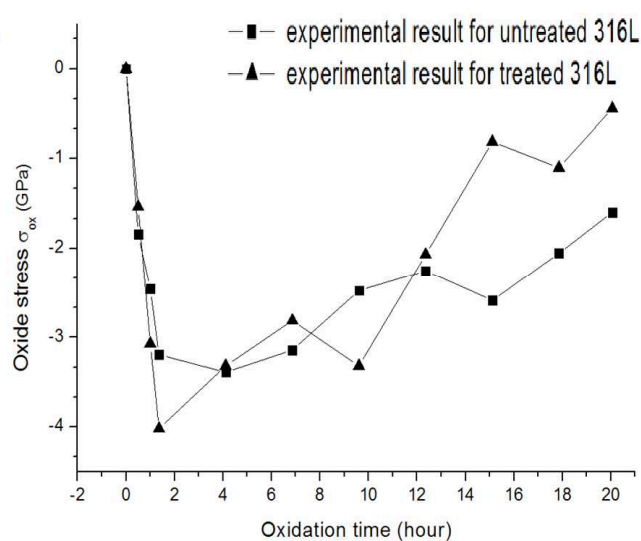


**Figure 6** Oxide stress versus oxidation time for untreated and treated 316L

At the beginning, the system is spontaneously able to generate increasing compressive stress in the oxide film during its growth. Strain incompatibility between metal and oxides is responsible for tensile stress in the alloy and generates in response compressive stress in the growing oxide. In a second stage, the stress level decreases because of the relaxation phenomena. The shape of these curves is in agreement with previous experimental results obtained during isothermal oxidation for other metal/oxide systems,  $\text{Fe}_2\text{O}_3/\text{Fe}_3\text{O}_4/\text{Fe}$  [9], and  $\text{Cr}_2\text{O}_3/\text{NiCr}_{30}$  [10]. The two presented curves are relatively similar with few differences. The average minimum value is around -3.5 GPa and the relaxation time value is about 3h. After relaxation (all along the oxidation time), the stress reached in the oxide film is smaller for treated samples, which means higher amplitude of relaxation in this case. This difference can be explained by the fact that the characteristic relaxation time depends on Young modulus of the oxide [11].

## Conclusion

In the present work, different experiments have been performed on nanocrystallised 316L stainless steel. High temperature oxidation of this alloy has been studied with both macroscopic and mesoscopic experiments. Specific mass gain measurements after 20 h of oxidation at 650°C indicated that the mass gain of the treated 316L material was significantly higher than that of the untreated material. For all studied samples, XRD and Raman spectroscopy results reveal the presence of three main oxide phases:  $\text{Fe}_2\text{O}_3$ ,  $\text{Fe}_3\text{O}_4$  and  $\text{Cr}_2\text{O}_3$ , which are present in the protective oxide layer. In-situ Raman measurements have been presented to show the stress evolution in samples with oxidation time, taking into account the calibration dependence of wavenumbers with temperature. Mechanical features associated to both the compressive stress and the creep relaxation phenomena occurring in the  $\text{Cr}_2\text{O}_3$  growing on 316L alloy system have been determined for both untreated and SMATed samples.

## References

- [1] T. Roland, D. Retraint, J. Lu, K. Lu, Mater. Sci. Forum 490-491 (2005) 625-630.
- [2] J. Uusitalo, L.P. Karjalainen, D. Retraint, M. Palosaari, Fatigue Properties of Steels with Ultrasonic Attrition Treated Surface Layers, Mater. Sci. Forum 604-605, (2009) 239-248.
- [3] T. Balusamy, S. Kumar, T.S.N. Sankara Narayanan, Corros. Sci. 52 (11) (2010) 3826-3834.

- 
- [4] J. Pitter, F. Cerny, J. Cizner, J. Suchanek, D. Tischler, Surf. Coat. Tech. 200 (2005) 73.
- [5] D. Retraint, C. Pilé, C. Garnier, J. Lu, 2nd edition, Society for Experimental Mechanics, vol. 1, (2005). p. 146.
- [6] H. Buscail, S. El Messki, F. Riffard, S. Perrier, R. Cueff, E. Caudron, C. Issartel Materials Chemistry and Physics 111 (2008) 491–496
- [7] M. Kemdehoundja, Analyse par microspectroscopie Raman de l'évolution des contraintes de croissances et résiduelles au cours de la formation de films de chromine sur l'alliage Ni-30Cr. Thèse de doctorat, Université de La Rochelle (2008)
- [8] J. Mougin, T. Le Bihan, G. Lucazeau, J. Phys. Chem Solids, 62 (2001) 553-563
- [9] B. Panicaud, J.L. Grosseau-Poussard, P.O. Renault, J.F. Dinhut, D. Thiaudière, M. Gailhanou, Appl. Surf. Sci. 206 (2003) 149–158.
- [10] B. Panicaud, J.L. Grosseau-Poussard, M. Kemdehoundja, J.F. Dinhut, Comput. Mater. Sci. 46 (2009) 42–48.
- [11] B. Panicaud, J.-L. Grosseau-Poussard, D. Retraint, M. Guérain, L. Li Corrosion Science 68 (2013) 263–274